Zitierweise:

doi.org/10.1002/anie.202303770

VIP Crystal Growth Very Important Paper

Multi-Step Nucleation of a Crystalline Silicate Framework via a Structurally Precise Prenucleation Cluster

*Biao Jin[+], Ying Chen[+], Jinhui Tao, Kacper J. Lachowski, Mark E. Bowden, Zihao Zhang, Lilo D. Pozzo, Nancy M. Washton, Karl T. Mueller, and James J. De Yoreo**

Abstract: Hierarchical nucleation pathways are ubiquitous in the synthesis of minerals and materials. In the case of zeolites and metal–organic frameworks, pre-organized multi-ion "secondary building units" (SBUs) have been proposed as fundamental building blocks. However, detailing the progress of multi-step reaction mechanisms from monomeric species to stable crystals and defining the structures of the SBUs remains an unmet challenge. Combining in situ nuclear magnetic resonance, small-angle X-ray scattering, and atomic force microscopy, we show that crystallization of the framework silicate, cyclosilicate hydrate, occurs through an assembly of cubic octameric Q^3_8 polyanions formed through cross-linking and polymerization of smaller silicate monomers and other oligomers. These Q^3_8 are stabilized by hydrogen bonds with surrounding H_2O and tetramethylammonium ions (TMA^+). When Q^3_8 levels reach a threshold of ≈32 % of the total silicate species, nucleation occurs. Further growth proceeds through the incorporation of $[(TMA)_x(Q^3_8)\cdot n\,H_2O]^{(x-8)}$ clathrate complexes into step edges on the crystals.

[*] Dr. B. Jin,[+] Y. Chen,[+] J. Tao, M. E. Bowden, Z. Zhang, N. M. Washton, K. T. Mueller, J. J. De Yoreo
Physical Sciences Division, Pacific Northwest National Laboratory
Richland, WA 99352 (USA)
E-mail: James.DeYoreo@pnnl.gov

Dr. K. J. Lachowski
Molecular Engineering and Sciences Institute, University of Washington
Seattle, WA 98105 (USA)

Dr. L. D. Pozzo
Department of Chemical Engineering, University of Washington
Seattle, WA 98105 (USA)

J. J. De Yoreo
Department of Materials Science and Engineering, University of Washington
Seattle, WA 98105 (USA)

[+] These authors contributed equally to this work.

Introduction

Of the numerous multi-step nucleation pathways that have been reported,[1] those involving the assembly of oligomeric units that exist as stable solution species—often referred to as prenucleation clusters (PNCs)[2]—are amongst the most difficult to confirm and thus the most controversial.[3] In some cases, PNCs are reported to be minor species in solutions that are otherwise dominated by monomeric species, but the PNCs, nonetheless, define the building unit of the growing nucleus.[4] In other instances, PNCs are claimed to be the dominant form of the solution species and are far in excess of classical expectations for the cluster size distribution at equilibrium,[2a] with a positive change in entropy associated with the release of waters of hydration implicated as the underlying source of this excess.[5]

Regardless of their concentration, in general, crystallization from PNCs has been reported to progress via an indirect route in which these disordered, dynamic species aggregate to form a bulk highly disordered or amorphous phase (liquid or solid) prior to the appearance of the crystalline phase, which often differs in composition, requiring a chemical evolution to accompany crystallization. The dominance of this multistep pathway is typically attributed to the replacement of a single large barrier to nucleation associated with the direct assembly of monomeric units by two smaller barriers—one to form the amorphous phase and a second to form the crystalline phase—with the first barrier rendered smaller still by aggregating the oligomeric PNCs in place of the monomeric species.[1]

Attempts to quantitatively probe PNCs and their assembly have been largely limited to relatively simple lattices of ionic species, such as calcium carbonate,[2a] calcium phosphate,[4b] and iron oxide.[6] Yet some of the earliest evidence for nucleation from oligomeric precursors was reported for far more complex, hierarchical structures, particularly porous silicate frameworks, such as zeolites,[7] in which the lattice consists of an ordered arrangement of multi-ion subunits, often possessing organic constituents that serve to stabilize the open framework. What has remained unclear, is whether nucleation of these frameworks occurs by the gradual collective ordering of a network of monomeric species, or whether the subunits—so-called "secondary building units" (SBUs)—are first constructed and then act as PNCs that directly assemble into the crystal phase. Thus, while the presence of oligomeric units in various zeolite-forming systems is now widely reported, the exis-

tence of prefabricated building units that assemble sequentially to form the crystal is still unproven.[8]

Similar questions apply to the nucleation of other classes of open framework lattices, including metal–organic frameworks (MOFs), covalent organic frameworks (COFs), and those constructed from polyhedral oligomeric silsesquioxanes (POSS).[9] Establishing a fundamental understanding of how order emerges in this important class of solids—and thus developing strategies to manipulate the onset and progression of crystallization—is of particular importance given the wide range of pressing technological challenges to which they can be applied, such as green catalysis, CO_2 capture, hydrogen storage, molecular separation, and drug delivery.[10]

Here we attempt to answer the above questions by directly observing the ladder of molecular assembly events that leads to the crystallization of cyclosilicate hydrate $\{[(CH_3)_4N]_8[Si_8O_{20}]\cdot 65\,H_2O\}$, which is a POSS-based silicate framework in which a cuboidal octameric polyanion $Si_8O_{20}^{8-}$ (designated as $Q^3{}_8$) coordinated to H_2O and trimethyl ammonium cations ($(CH_3)_4N^+$, TMA^+) defines the SBU (Figure 1). We do so by using in situ nuclear magnetic resonance (NMR) and small-angle X-ray scattering (SAXS) to monitor the structural and dynamical evolution of various silicate species during crystallization and liquid-phase atomic force microscopy (AFM) to follow post-nucleation cyclosilicate hydrate growth. Previous work using in situ NMR on undersaturated solutions confirmed that $Q^3{}_8$ units comprise stable solution species that form from smaller species (Q^0, $Q^1{}_2$, $Q^2{}_3$, and $Q^3{}_6$) with which they remain in equilibrium.[11] However, whether or not those units play a role in nucleation, which species controls the induction time and why, and how each is involved in the post-nucleation growth process remained unresolved.

The results presented here, which are obtained on supersaturated solutions, demonstrate that the $Q^3{}_8$ unit is indeed the dominant cage-like silicate species in the solutions at the time of nucleation. In fact, the induction time is determined by the time point at which the concentration of these units exceeds a specific value. Thus, the saturation state relative to cyclosilicate hydrate is defined in terms of the $Q^3{}_8$ activity, not that of the monomers. Moreover, with increasing $Q^3{}_8$ concentration, ion-rich regions are formed comprising a large network of $[(TMA)_x(Q^3{}_8)\cdot n\,H_2O]^{(x-8)}$ clathrate structures[11a] from which the nuclei emerge. Following nucleation, cyclosilicate hydrate crystals grow layer-by-layer through the advancement of steps with an average height that matches the unit cell dimension of the crystal, implying they grow through repeated addition of the SBUs. These findings provide a comprehensive picture of the multi-step crystallization pathway of this silicate framework from initial monomers to final crystal and show that nucleation proceeds through the direct assembly of a structurally uniform population of PNCs that are identical to the SBU of the framework.

Results and Discussion

All nucleation and growth experiments were done using aqueous solutions containing 1 M SiO_2 and 2 M TMAOH. After heating the solution at 60 °C followed by subsequent incubation at 25 °C, rhombohedral platelet-shaped crystals appeared (Figure 1b and Figure S1a) reaching sizes in the range of several tens' micrometers to millimeters. The existence of $Q^3{}_8$, H_2O, and TMA^+ in the crystals was revealed by attenuated total reflectance-Fourier transform infrared (ATR-FTIR) spectra (Figure S1b and thermogravimetric analysis-mass spectrometry (TGA-MS) (Figure S2), as well as ^{29}Si solid-state (SS-) NMR spectroscopy (Figure S3). Single crystal XRD (SC-XRD) further showed the atomic structure of the synthesized crystals, comprising $Q^3{}_8$ surrounded by TMA^+ and H_2O. The SC-XRD structure was the same as that published by Wiebcke et al.[12] and given the reference code YITGIR by the Cambridge Crystallographic Data Center. Moreover, high-resolution transmission electron microscopy (HR-TEM) and selected area electron diffraction (SAED) images confirmed the platelets were single-crystals of cyclosilicate hydrate (Figure 1a and S4).

To follow the structural evolution of solution species during nucleation of cyclosilicate hydrate crystals, we acquired time-resolved ^{29}Si and ^{1}H NMR spectra of solutions containing 1 M SiO_2 and 2 M TMAOH at 25 °C immediately after boiling the solution at 180 °C, which breaks down the most stable silicate oligomers into monomers. As shown in the ^{29}Si spectrum acquired for 55 hours (Figure S5), in addition to the five singlet signals from the dominating species with only a single silicon chemical environment (i.e., monomer Q^0, dimer $Q^1{}_2$, cyclic trimer $Q^2{}_3$, prismatic

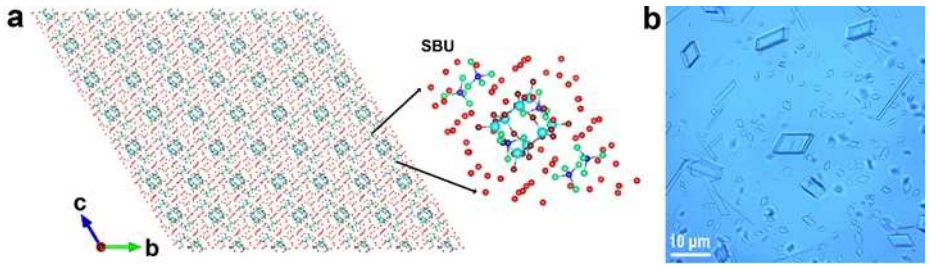

Figure 1. Structural characterization of cyclosilicate hydrate crystal. a) The left-hand panel shows a single crystal structure of $[TMA_8Q^3{}_8]\cdot 65\,H_2O$ determined from SC-XRD measurements. Sub-unit of the crystal that would naturally define the SBU is highlighted in the right-hand panel. b) Optical microscopy images showing rhombohedral or needle-like crystals of cyclosilicate hydrate in solution.

hexamer Q^3_6, and Q^3_8), there are multiple small signals arising from Q^2 and Q^3 units in some 3-ring or 4-ring structures, with some potential species listed that are consistent with the assignments by Knight et al.[13] Because it is impractical to identify and quantify these small signals individually at each time point, only the sum of these signals is reported.

From the NMR spectra (Figure 2a, S6 and S7), we quantified the time-dependent concentration of the various silicate species (Figure 2b, c). The results show that, as we observed previously in 1 M SiO_2 solutions containing only 1 M TMAOH, slow growth of Q^3_8 cages occurs at the expense of smaller silicate species.[11a] TEM analysis of drop-cast samples provides further support for this conclusion, demonstrating the existence of oligomers with an average size of 0.58 nm (Figure 2d, e), which roughly corresponds to the calculated size of Q^3_8.

During the initial period of Q^3_8 growth, the increase in the fraction of Q^3_8 cages is matched by the decrease in the fraction of Q^3_6 plus that of $Q^0+Q^1_2+Q^2_3$, demonstrating that Q^3_6 serves as a reaction intermediate for the creation of Q^3_8. However, unlike the lower concentration 1 M TMAOH solutions in which nucleation did not occur and solutions reached an equilibrium distribution of species for which Q^3_8 attained a fraction of 83 %,[11a] in these more concentrated 2 M TMAOH solutions, nucleation occurs when the Q^3_8 fraction crosses ≈32 %, at which point the Q^3_8 fraction plummets. This behavior shows that, in solutions with 2 M TMAOH, the relative concentrations of the various species are out of equilibrium, the activities of TMA^+ and Q^3_8 species, rather than the Q^0 monomers, define the super-saturation at which nucleation occurs, and the Q^3_8 species are directly consumed during the nucleation event.

The dramatic drop in the Q^3_8 fraction at the nucleation point is followed by a slower decrease (Figure 2b) as the newly formed crystals grow. This decrease in Q^3_8 is accompanied by a decrease in Q^3_6 and other 3-ring or 4-ring structures (Figure S6), while the amount of small silicate species (Q^0, Q^1_2, Q^2_3) remains almost unaltered. Interestingly, the concentration of Q^3_8 appears to plateau after 45 hours as the rate of Q^3_8 formation from the less stable species approaches the rate of Q^3_8 consumption due to

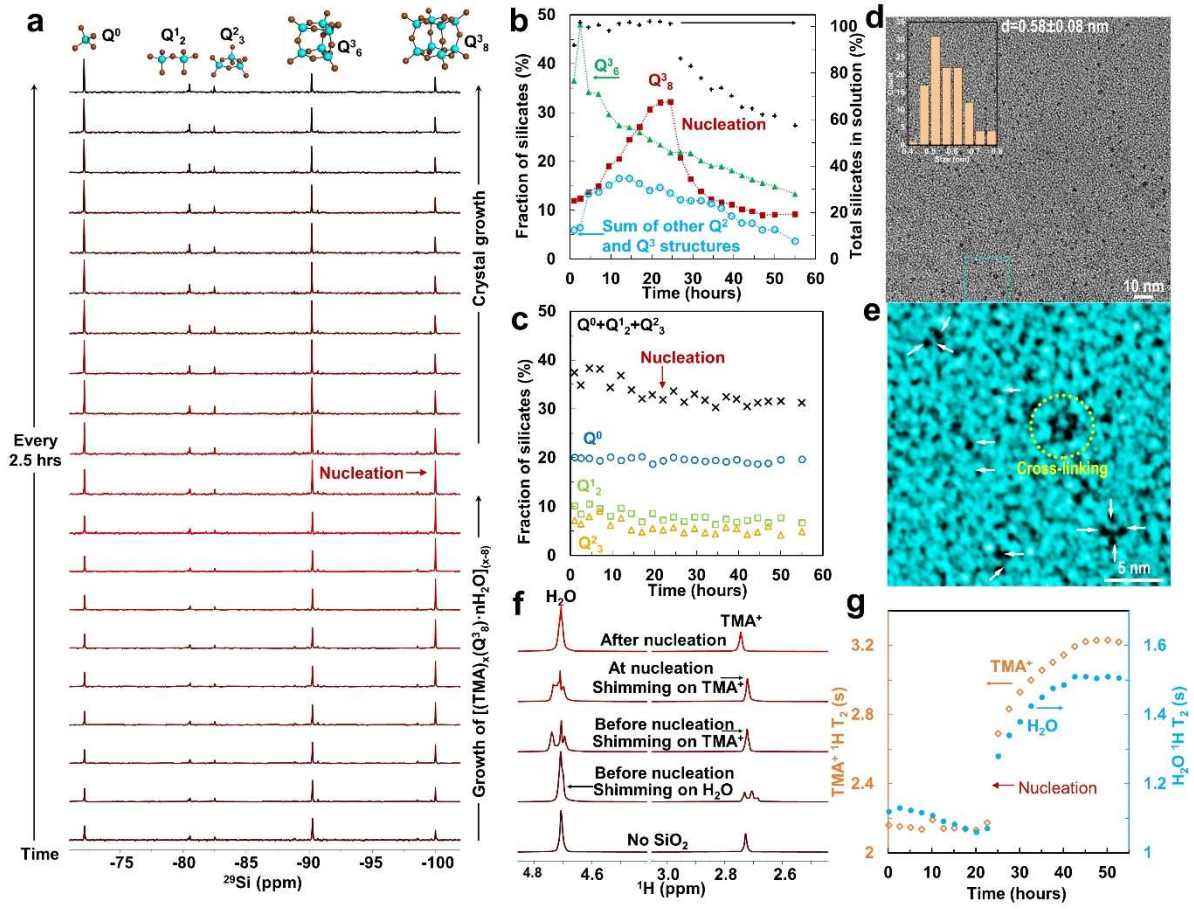

Figure 2. The formation process of cyclosilicate hydrate crystal. a) In situ liquid state ^{29}Si NMR spectra collected at an interval of 2.5 hours after boil-freeze-thaw treatment shows the evolution of silicate species during the crystallization process. b), c) The quantified evolution of different silicate species. These samples were taken from a prenucleation solution. d) TEM image of Q^3_8 units and corresponding size distribution (inset). e) Magnified TEM image with false color. f) ^1H NMR was collected before and after nucleation compared to the 2 M TMAOH solution with no SiO_2. g) ^1H T_2 of H_2O and TMA^+.

crystal growth. Having confirmed from ^{29}Si solid-state NMR and SC-XRD (Figure 1a, S3) that the crystal only consists of Q^3_8 units, these results imply that Q^3_6 and other ring structures continue to serve as a reservoir for the creation of Q^3_8, which in turn serves as the building unit for the growing crystal.

The NMR spectra also provide insight into the interactions of the Q^3_8 with water before and after nucleation. Prior to the nucleation, H_2O and TMA^+ surround the Q^3_8 and form hydrogen bonds with the terminal oxygen atoms of the Q^3_8 silicate cage, leading to the formation of $[(TMA)_x$-$(Q^3_8)\cdot n\,H_2O]^{(x-8)}$ clathrate structures. Post-nucleation, a stronger hydrogen bond between H_2O and TMA^+ with Q^3_8 is observed, as indicated by the down-field shifted ^{1}H NMR signals from the crystals (Figure S3b). By quantifying the integrated areas for ^{1}H NMR peaks of structural H_2O and TMA^+, the molar ratio of crystalline H_2O and TMA^+ in cyclosilicate hydrate is estimated to be $\approx$8.3. Given the stoichiometric ratio of $[TMA^+]$ to $[Q^3_8]$ (exactly 8), we determine the cyclosilicate hydrate formula to be $[N(CH_3)_4]_8[Si_8O_{20}](H_2O)_{66}$, which is almost in line with previously reported compositions.[12]

To understand the important role of the interactions between Q^3_8 and H_2O or TMA^+ in controlling the occurrence of nucleation, we probed the solution dynamics of H_2O and TMA^+ during the pre-and post-nucleation stage. As shown in Figure 2f, compared to the well-defined Lorentzian line shape of the proton signals from both TMA^+ and H_2O for the solution containing 2 M TMAOH (no SiO_2) or 1 M TMAOH and 1 M SiO_2, ^{1}H signals of the pre-nucleation solution containing 2 M TMAOH and 1 M SiO_2 exhibit poor resolution. More specially, when the H_2O resonance is shimmed to achieve high resolution, the TMA^+ signal displays multiple peaks spreading over 0.1 ppm, and vice versa. This abnormal phenomenon strongly suggests that the majority of TMA^+ and the bulk water in the pre-nucleation solution are in two distinctive environments with structural heterogeneity. As reported in our previous work,[11a] Q^3_8 units are stabilized by $[(TMA)_x(Q^3_8)\cdot n\,H_2O]^{(x-8)}$ clusters in the solution of 1 M TMAOH and 1 M SiO_2. The results imply that, upon increasing the TMAOH concentration to 2 M, the increase in the Q^3_8 concentration is accompanied by the formation of large, interconnected networks consisting of $[(TMA)_x(Q^3_8)\cdot n\,H_2O]^{(x-8)}$ clusters. Given that TMA^+ and Q^3_8 in solution are fully detectable by liquid-state ^{1}H and ^{29}Si NMR prior to nucleation, these networks are definitely in a liquid state and the constituent species have high mobility suggesting they comprise a dense liquid phase and further highlighting the nonclassical nature of the nucleation process. The ^{1}H NMR resolution improves significantly right after nucleation and returns to a normal, well-resolved line shape 5 hours after nucleation. Meanwhile, the decrease in the Q^3_8 fraction slows down after 5 hours, indicating that all pre-existing $TMA\cdot Q^3_8$ are depleted, and the slow crystal growth is enabled by new $[(TMA)_x(Q^3_8)\cdot n\,H_2O]^{(x-8)}$ clusters freshly formed at an expense of the Q^3_6 and other large ring structures.

Measurements of the self-diffusion coefficients (D, Figure S8a), ^{1}H spin-lattice relaxation (T_1, Figure S8b), and spin-spin relaxation time constants (T_2, Figure 2g) of H_2O and TMA^+ further highlight the distinct mesoscale environment in which nucleation takes place. The initial slight drop in D and T_2 of TMA^+ and H_2O may be attributed to some TMA^+ and H_2O associated with silicate polyanions as ion complexes and the exchange of TMA^+ and H_2O between the bulk and ion-rich regions. Once the concentration of Q^3_8 reaches a threshold value (32 % in solution corresponds to 0.04 M) in the 2 M TMAOH solution, nucleation occurs within the ion-rich regions, causing the TMA^+ and H_2O molecules that are associated with Q^3_8 units to precipitate from the solution. The remaining solution has a much smaller viscosity, therefore D, T_1, and T_2 all experience a sudden increase after nucleation and continue to increase during crystal growth.

To obtain independent in situ data on the development of SBUs, time-resolved SAXS was used to characterize structural changes during the nucleation and growth of cyclosilicate hydrate after heating a sample in a sealed glass NMR tube overnight at 60 °C (Figure 3). The time-resolved data are well fit by a model consisting of the product of a spherical form factor and hard-sphere structure factor (Figure 3b). The form factor represents scattering contributions from cyclosilicate species, and the structure factor approximates their interactions with one another. Four hours after removal from the oven, the prominence of the peak in the scattering curve due to interparticle interactions and the overall intensity of the feature decreased due to the precipitation of crystalline material. The crystallinity of the precipitate was verified using SAXS/WAXS measurements (Figure 3d) collected at the bottom of the NMR tube. The liquid upper phase, on the other hand, showed no evidence of crystallinity.

The particle radius ($\approx$0.45 nm) and effective hard-sphere radius ($\approx$0.72 nm) obtained from the data (Figure 3b) are consistent with the size of cyclosilicate species plus the approximate extent of the shell of TMA^+ and H_2O that surrounds them, respectively. The two radii are initially constant, but a slight decrease is observed around 4 hours. Both Q^3_8 and Q^3_6 species can contribute to this feature, but Q^3_6 is slightly smaller. Therefore, the slight decrease in radius is consistent with the hypothesis that Q^3_8 is a building unit for the observed crystals, and that Q^3_6 makes up a larger fraction of the suspended cyclosilicate species after nucleation of the crystals. Due to the lack of information about the exact scattering length densities of silicate species and the surrounding medium, the value of the volume fraction is arbitrary. Nevertheless, changes in the scattering invariant (Q) (Figure 3c) are proportional to changes in the volume fraction of particles in a suspension. The trend in the invariant is consistent with the rapid decrease of Q^3_8 after nucleation, followed by a slow decay (Figure 2b).

To obtain independent in situ data on the incorporation of SBUs into the growing crystals following nucleation, we directly observed cyclosilicate hydrate post-nucleation growth in aqueous solutions using liquid phase AFM (Figure 4, see method for details). The results show that the crystal surface consists of steps and step bunches separated by micrometer-wide terraces lacking obvious defects (Fig-

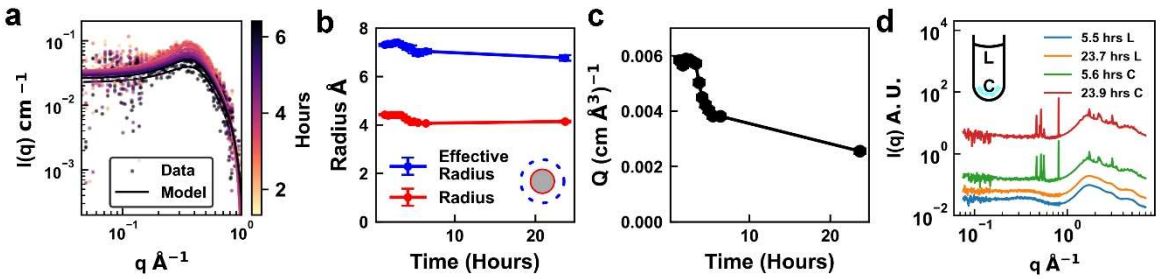

Figure 3. In situ SAXS tests. a) SAXS measurements of the upper, liquid phase in the NMR tube were taken at different time points after removal from the oven. Note that the last scattering profile with the lowest intensity corresponds to the measurement taken after 23 hours. A sudden decrease in intensity was identified around 4 hours. Data were fitted with a sphere form factor and a hard sphere structure factor. b) The radius from the sphere form factor model and the effective radius of the hard sphere model remained relatively constant. c) The scattering invariant (Q), which is proportional to the volume fraction of all scatterers, is plotted over time. Note the sudden decrease at 4 hours which indicates the formation of the crystalline precipitate. d) Arbitrarily scaled scattering and diffraction were measured in the bottom crystal phase (C) and the top liquid phase (L) of the sample at two different time points. Changes in the upper phase of the sample indicate a decrease in the concentration of silicate species, and no crystallinity is observed due to sedimentation to the bottom crystalline phase. Crystalline precipitate was visually observed and characterized using SAXS in the crystalline phase after the intensity in the upper phase began to decrease.

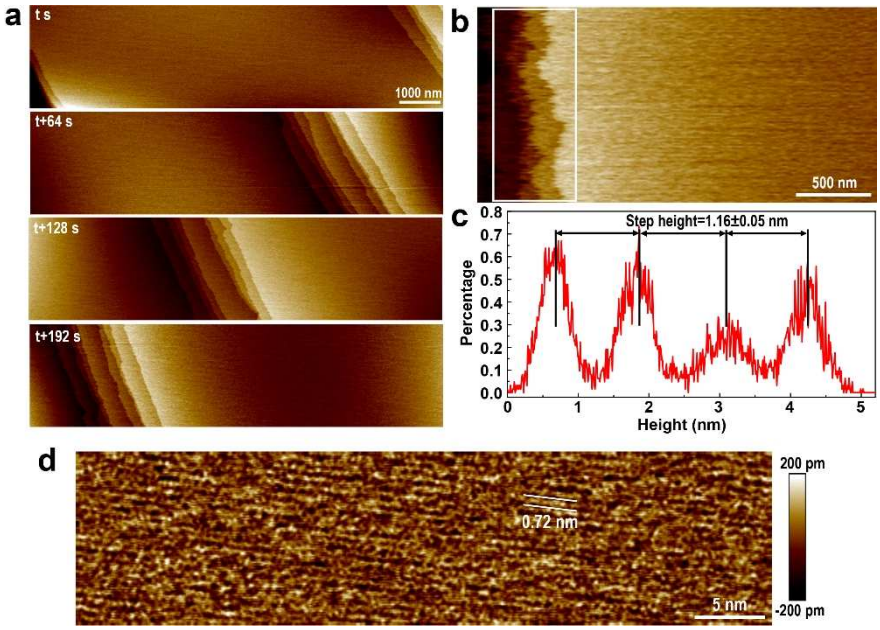

Figure 4. In situ liquid phase AFM observations of unfinished layer growth on the crystal surface. a) Time-resolved in situ AFM height images show the growth process of multiple steps in a highly alkaline solution. b) AFM image shows the topography of crystal surface with multiple steps at the edge. c) The graph shows the height distribution in the area marked in "b", giving a height difference of 1.16 ± 0.05 nm between adjacent steps. d) High-resolution AFM images reveal the locally ordered structure. The lattice distance of 0.72 nm is identified.

ure 4a). The source of the steps—two-dimensional nucleation of islands or propagation from a screw dislocation—is unknown, but the observed step bunching suggests the latter, as it is a common phenomenon for step trains far from a dislocation source due to either impurity inhibition of step growth[14] or instabilities arising from inadequate mass transport in unmixed solutions (as were used here).[15] Step speeds were determined to be 42 nm s^{-1} (Figure S9). The growing step-edges (Figure 4b) are extremely rough, presenting a high kink density for the attachment of growth units and implying a kink energy of order $k_B T$ or less (where k_B is Boltzmann's constant) which is consistent with the highly hydrated nature of the lattice. The step height is 1.16 ± 0.05 nm (Figure 4c), which is similar to the diameter of the cyclosilicate species and a surrounding shell of TMA^+ and H_2O determined from the in situ SAXS measurements discussed above, as also reported before.[16] The highest step (≈1.2 nm) corresponds to the length of one side of a unit cell (1.2273 nm) of cyclosilicate hydrate and high-resolution imaging on the terraces (Figure 4d) reveals a 0.72 nm periodicity of the surface lattice, which coincides well with the diagonal (0.7201 nm) of a Q^3_8 unit.[17] These observations reveal a two-dimensional layer-by-layer growth mechanism wherein new crystal layers nucleate and grow by the attach-

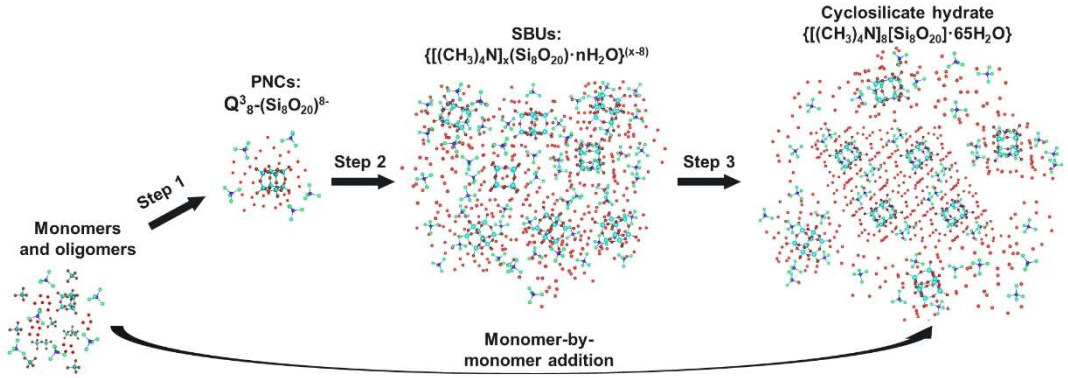

Scheme 1. The proposed three-step crystallization mechanism for cyclosilicate hydrate. Step 1 is the formation of Q^3_8 from smaller silicate monomers and oligomers; Step 2 is the prenucleation stage where ion-rich regions are formed with a large network of $\{[(TMA)_x(Q^3_8)\cdot n\,H_2O]^{(x-8)}\}_n$ clathrate structures due to additional TMA^+; Step 3 is the ordered self-assembly of the pre-organized complex into a well-defined single-crystalline cyclosilicate hydrate. The classical pathway of monomer-by-monomer addition is also highlighted at the bottom as it may occur to some degree, but was not detected in our experiments.

ment of growth units at the step edges exhibiting dimensions consistent preassembled $[(TMA)_x(Q^3_8)\cdot n\,H_2O]^{(x-8)}$ SBUs. Layer-by-layer growth through the addition of oligomeric building units was also reported for zeolite crystallization.[18]

Conclusion

The findings presented above define a crystallization pathway for cyclosilicate hydrate crystals that begins with the formation of structurally precise, stable PNCs that comprise the SBU of this framework lattice (Scheme 1) through the association of silicate monomers or smaller silicates and TMA^+ (Step 1). This path is distinct from classical monomer-by-monomer attachment, although the latter may well occur concurrently at a level too small to be detectable by a drop in the Q^0 NMR signal. During the pre-nucleation period, the pre-organization of Q^3_8 with H_2O and TMA^+ into $[(TMA)_x(Q^3_8)\cdot n\,H_2O]^{(x-8)}$ clathrate structures as SBUs, further drives the formation of ion-rich regions containing a large network of $\{[(TMA)_x(Q^3_8)\cdot n\,H_2O]^{(x-8)}\}_n$ clathrate structures (Step 2). Following that, the nucleation of cyclosilicate hydrate occurs (Step 3) through the ordered self-assembly of the SBUs into a well-defined single-crystalline cyclosilicate hydrate, accompanied by the rearrangement of H_2O and TMA^+. During the post-nucleation growth stage, the SBUs and H_2O are incorporated into the crystal surface, driving the continuous growth into a micro-scale size crystalline structure. The developed crystallization model through direct observation of structurally precise PNCs and SBUs as well as their transition into crystals complements the conceptual understanding of the multi-step nucleation mechanism, paving a road towards understanding the synthesis mechanism of porous framework crystals, with broad implications for the synthesis of functional materials ranging from adsorbents and catalysts to photovoltaics and semiconductors, as well as natural minerals.

Acknowledgements

This research was performed at Pacific Northwest National Laboratory (PNNL) with support from the U.S. Department of Energy (DOE), Office of Science (SC), Basic Energy Sciences (BES), Division of Materials Sciences and Engineering, under Award FWP67554. PNNL is operated by Battelle for the U.S. DOE under contract no. DE-AC05-76RLO1830. NMR, ATR-FTIR, XRD, SEM, and high-resolution TEM tests were performed under user proposals 60243 and 50824 at the Environmental Molecular Sciences Laboratory (EMSL), which is a DOE, SC, Office of Biological and Environmental Research user facility located at PNNL. SAXS measurements were supported by the U.S. DOE, SC, BES, as part of the Energy Frontier Research Centers program: CSSAS—The Center for the Science of Synthesis Across Scales—under Award DE-SC0019288. This work also benefited from the use of the SasView application, originally developed under NSF award DMR-0520547. SasView also contains code developed with funding from the European Union's Horizon 2020 research and innovation program under the SINE2020 project, grant agreement No 654000. The authors acknowledge the use of facilities and instrumentation supported by the U.S. National Science Foundation through the Major Research Instrumentation (MRI) program (DMR-2116265) and the UW Molecular Engineering Materials Center (MEM·C), a Materials Research Science and Engineering Center (DMR-1719797).

Conflict of Interest

The authors declare no competing financial interests.

Data Availability Statement

The data that support the findings of this study are available in the Supporting Information of this article.

Keywords: Cyclosilicate Hydrate · Multi-Step Nucleation · Polyanions · Prenucleation Clusters · Self-Assembly

[1] J. J. De Yoreo, P. U. Gilbert, N. A. Sommerdijk, R. L. Penn, S. Whitelam, D. Joester, H. Zhang, J. D. Rimer, A. Navrotsky, J. F. Banfield, A. F. Wallace, F. M. Michel, F. C. Meldrum, H. Cölfen, P. M. Dove, *Science* **2015**, *349*, aaa6760.
[2] a) D. Gebauer, A. Volkel, H. Colfen, *Science* **2008**, *322*, 1819–1822; b) D. Gebauer, M. Kellermeier, J. D. Gale, L. Bergström, H. Cölfen, *Chem. Soc. Rev.* **2014**, *43*, 2348–2371.
[3] a) K. Henzler, E. O. Fetisov, M. Galib, M. D. Baer, B. A. Legg, C. Borca, J. M. Xto, S. Pin, J. L. Fulton, G. K. Schenter, *Sci. Adv.* **2018**, *4*, eaao6283; b) P. J. Smeets, A. R. Finney, W. J. Habraken, F. Nudelman, H. Friedrich, J. Laven, J. J. De Yoreo, P. M. Rodger, N. A. Sommerdijk, *Proc. Natl. Acad. Sci. USA* **2017**, *114*, E7882–E7890.
[4] a) N. A. Garcia, R. I. Malini, C. L. Freeman, R. Demichelis, P. Raiteri, N. A. Sommerdijk, J. H. Harding, J. D. Gale, *Cryst. Growth Des.* **2019**, *19*, 6422–6430; b) W. J. Habraken, J. Tao, L. J. Brylka, H. Friedrich, L. Bertinetti, A. S. Schenk, A. Verch, V. Dmitrovic, P. H. Bomans, P. M. Frederik, *Nat. Commun.* **2013**, *4*, 1507.
[5] M. Kellermeier, P. Raiteri, J. K. Berg, A. Kempter, J. D. Gale, D. Gebauer, *ChemPhysChem* **2016**, *17*, 3535–3541.
[6] J. Scheck, M. Drechsler, X. Ma, M. Stöckl, J. Konsek, J. B. Schwaderer, S. Stadler, J. J. De Yoreo, D. Gebauer, *J. Chem. Phys.* **2016**, *145*, 211917.
[7] S. L. Burkett, M. E. Davis, *J. Phys. Chem.* **1994**, *98*, 4647–4653.
[8] S. Hong, A. J. Mallette, J. J. Neeway, R. K. Motkuri, J. D. Rimer, G. Mpourmpakis, *Dalton Trans.* **2023**, *52*, 1301–1315.
[9] a) N. Pellens, N. Doppelhammer, S. Radhakrishnan, K. Asselman, C. V. Chandran, D. Vandenabeele, B. Jakoby, J. A. Martens, F. Taulelle, E. K. Reichel, E. Breynaert, C. E. A. Kirschhock, *Chem. Mater.* **2022**, *34*, 7139–7149; b) L. Kollias, R. Rousseau, V.-A. Glezakou, M. Salvalaglio, *J. Am. Chem. Soc.* **2022**, *144*, 11099–11109; c) M. Huang, C.-H. Hsu, J. Wang, S. Mei, X. Dong, Y. Li, M. Li, H. Liu, W. Zhang, T. Aida, *Science* **2015**, *348*, 424–428.
[10] a) H. Shi, J. Yang, M. You, Z. Li, C. He, *ACS Mater. Lett.* **2020**, *2*, 296–316; b) W. Chaikittisilp, M. Kubo, T. Moteki, A. Sugawara-Narutaki, A. Shimojima, T. Okubo, *J. Am. Chem. Soc.* **2011**, *133*, 13832–13835.
[11] a) Y. Chen, N. M. Washton, R. P. Young, A. J. Karkamkar, J. J. De Yoreo, K. T. Mueller, *Phys. Chem. Chem. Phys.* **2019**, *21*, 4717–4720; b) S. D. Kinrade, C. T. G. Knight, D. L. Pole, R. T. Syvitski, *Inorg. Chem.* **1998**, *37*, 4272–4277; c) S. D. Kinrade, C. T. G. Knight, D. L. Pole, R. T. Syvitski, *Inorg. Chem.* **1998**, *37*, 4278–4283.
[12] M. Wiebcke, M. Grube, H. Koller, G. Engelhardt, J. Felsche, *Microporous Mater.* **1993**, *2*, 55–63.
[13] C. T. G. Knight, R. G. Balec, S. D. Kinrade, *Angew. Chem. Int. Ed.* **2007**, *119*, 8296–8300.
[14] a) L. Rashkovich, N. Kronsky, *J. Cryst. Growth* **1997**, *182*, 434–441; b) T. Thomas, T. Land, W. Casey, J. DeYoreo, *Phys. Rev. Lett.* **2004**, *92*, 216103; c) M. Ranganathan, J. D. Weeks, *J. Cryst. Growth* **2014**, *393*, 35–41.
[15] a) S. Coriell, B. Murray, A. Chernov, G. McFadden, *J. Cryst. Growth* **1996**, *169*, 773–785; b) N. A. Booth, A. A. Chernov, P. G. Vekilov, *Phys. Rev. E* **2004**, *69*, 011604.
[16] R. M. Laine, *J. Mater. Chem.* **2005**, *15*, 3725–3744.
[17] S. Sugiyama, S. Yamamoto, O. Matsuoka, H. Nozoye, J. Yu, G. Zhu, S. Qiu, O. Terasaki, *Microporous Mesoporous Mater.* **1999**, *28*, 1–7.
[18] M. Kumar, M. K. Choudhary, J. D. Rimer, *Nat. Commun.* **2018**, *9*, 2129.

Manuscript received: March 15, 2023
Accepted manuscript online: May 5, 2023
Version of record online: ■■, ■■

Forschungsartikel

Crystal Growth

B. Jin, Y. Chen, J. Tao, K. J. Lachowski, M. E. Bowden, Z. Zhang, L. D. Pozzo, N. M. Washton, K. T. Mueller, J. J. De Yoreo* _____ **e202303770**

Multi-Step Nucleation of a Crystalline Silicate Framework via a Structurally Precise Prenucleation Cluster

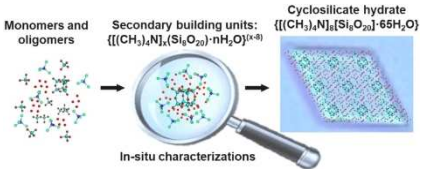

In situ characterizations reveal a multi-step crystallization pathway for cyclosilicate hydrate crystals that starts with the formation of structurally precise prenucleation clusters, which comprise the secondary building units of this framework lattice.